

Article

Not peer-reviewed version

Evaluation of Ocean Color Algorithms to Retrieve Chlorophyll-A Concentration in the Mexican Pacific Ocean off the Baja California Peninsula, Mexico

[Patricia Alvarado-Graef](#) , [Beatriz Martin-Atienza](#) ^{*} , Ramón Sosa-Ávalos , [Dr. Reginaldo Durazo](#) , Rafael Hernandez-Walls

Posted Date: 29 March 2024

doi: 10.20944/preprints202403.1809.v1

Keywords: Remote sensing; algorithms; ocean color; Chlorophyll-a



Preprints.org is a free multidiscipline platform providing preprint service that is dedicated to making early versions of research outputs permanently available and citable. Preprints posted at Preprints.org appear in Web of Science, Crossref, Google Scholar, Scilit, Europe PMC.

Copyright: This is an open access article distributed under the Creative Commons Attribution License which permits unrestricted use, distribution, and reproduction in any medium, provided the original work is properly cited.

Article

Evaluation of Ocean Color Algorithms to Retrieve Chlorophyll-a Concentration in the Mexican Pacific Ocean off the Baja California Peninsula, Mexico

Patricia Alvarado-Graef ¹, Beatriz Martín-Atienza ^{1,*}, Ramón Sosa-Ávalos ², Reginaldo Durazo ¹ and Rafael Hernández-Walls ¹

¹ Facultad de Ciencias Marinas, Universidad Autónoma de Baja California, Ensenada 22860, México; alvaradograef@uabc.edu.mx, atienza@uabc.edu.mx, rdurazo@uabc.edu.mx, rwalls@uabc.edu.mx

² Centro Universitario de Investigaciones Oceanológicas, Universidad de Colima, Manzanillo, 28060, México; rsosa@ucol.mx

* Correspondence: atienza@uabc.edu.mx ; Tel.: +52-646-1528213

Abstract: Mathematical algorithms relate satellite data of ocean color with the surface Chlorophyll-*a* concentration (Chl-*a*), a proxy of phytoplankton biomass. These mathematical tools work best when they are adapted to the unique bio-optical properties of a particular oceanic province. Ocean color algorithms should also consider that there are significant differences between datasets derived from different sensors. Common solutions are to provide different parameters for each sensor or use merged satellite data. In this paper we use satellite data from the Copernicus merged product suite and in situ data from the southernmost part of the California Current System to test two widely used global algorithms, OCx and CI, and a regional algorithm, CalCOFI2. The OCx algorithm gave the best result, therefore, it was regionalized and, again, tested. The database was then separated according to (a) dynamic boundaries in the area, (b) bio-optical properties and (c) climatic condition (El Niño/La Niña). Regional algorithms were obtained and tested for each partition. The Chl-*a* retrievals for each model were tested and compared. The best fit for the data was for the regional algorithms that considered the climatic conditions (El Niño/La Niña). These results will allow the construction of consistent regionally adapted time-series and, therefore, demonstrates the importance of El Niño/La Niña events on the bio-optical properties of the area.

Keywords: chlorophyll-*a*; remote sensing; ocean color algorithms; el niño – southern oscillation (ENSO)

1. Introduction

Oceanic ecosystems, haven to vast biodiversity, essential for climate regulation and provider of diverse benefits to humanity, are intricate systems. To comprehend their dynamics, we must monitor oceanographic variables consistently. Long time series with adequate spatial resolution are required in order to understand these complex ecosystems. While ship-based monitoring offers precise results, its infrequent coverage and high costs limit its efficacy. Moored or remotely operated instruments are an alternative, but they are spatially restricted. Satellite-derived data, on the other hand, provides expansive temporal coverage, albeit primarily for surface variables. Despite its coarser spatial resolution, it encompasses a vast majority of the ocean surface.

Satellite sensors, with their diverse optical bands, sensitivities, and overpass times [1], produce data that can vary significantly between sensors [2,3]. Such variations arise from differences in sensor characteristics and inherent uncertainties in calibration and even with the processing algorithms [4]. The parameters used in the algorithms are particular to each sensor [5]. Because of all of these facts, continuous climate data records cannot be constructed [6].

To enhance the satellite data's time coverage and, therefore, provide consistent time series, merging of data from different sensors becomes imperative [2,7,8]. Operational satellite sensor constellations, such as Copernicus, provide ocean color data as elements of an integrated, sustained

observing system [8] that has better global coverage and allow the study of phenomena of larger timescale than what an individual sensor provides [3]. The efficacy of such merged data must be regionally validated to ensure the algorithms used are optimal.

Bio-optical algorithms that relate ocean surface Chlorophyll-*a* concentration (Chl-*a*) with satellite data, are predominantly empirical, deriving their parameters from in situ data [9]. Level-3 Chl-*a* images available in the NASA Ocean Color Web Site employ an OCx algorithm merged with the color index algorithm (CI) [10] with different parameters for different sensors [5]. However, these global algorithms might not be regionally optimal [6]. For instance, some algorithms underestimate the values of Chl-*a* in the California Current area [6,11], while others overestimate them in the Northern Bering Sea and Chukchi Sea [12,13]. Thus, evaluating global algorithms' performance at regional levels becomes paramount, especially when using merged satellite data. Such evaluations pave the way for robust, long-term data series, enhancing our understanding and management of ocean ecosystems.

This research aims to evaluate various bio-optical algorithms for the Southern part of the California Current System (CCS), offshore the Baja California peninsula, and, if need be, provide a regionally optimal working algorithm. The CCS, a region known for its coastal upwelling, eddies, and fronts, has been under scrutiny since 1949 via the California Cooperative Oceanic Fisheries Investigations (CalCOFI) program focusing on the California coast, and since 1997 via the Mexican Research Program of the California Current (IMECOCAL) which centers on the region off the coast of Baja California. This region is a unique transitional zone where colder subarctic waters mingle with warmer tropical and subtropical currents [15,16]. This confluence, along with factors like circulation and water mass mixing, dictates the region's biological and chemical processes [17,18]. In particular, the mixture and the upwelling of nutrients determine the characteristics of the ecosystem [14,15,17,18]. Furthermore, interannual variations such as El Niño – Southern Oscillation (ENSO) strongly influence this intricate transitional ecosystem.

Our study assesses the efficacy of two global algorithms (OCx, CI) and a CCS-specific algorithm [9] using in situ Chlorophyll-*a* measurements off the Baja California Peninsula and Copernicus merged satellite data. The significance of this evaluation stems from the fact that the performance of Chl-*a* algorithms for Copernicus data in this region remains untested. Copernicus, with its merged sensor data, offers enhanced spatial and temporal coverage, enabling a deeper dive into regional processes, for example, the longer-term trends modulating atmosphere-ocean interactions in Eastern Boundary Upwelling Systems triggered by decadal-scale fluctuations linked to climate forcing [19].

Post evaluation, we propose and test a regionalization tailored for this area and satellite dataset. To refine our understanding, we segmented the dataset based on hydrographic properties, bio-optical properties, and climatic events like ENSO. For each segment, specific algorithms were introduced and evaluated. Our findings facilitate the selection of the most representative model for this region using the Copernicus dataset, shedding light on the region's distinct bio-optical properties. A meticulously analyzed Chl-*a* retrieval from a consistent dataset across instruments will bolster our understanding of biogeochemical processes and the broader implications of climate change.

2. Methodology

In this section we describe the methodology used to estimate Chl-*a* from satellite data in the IMECOCAL region. We initiate with the application of a global algorithm to the remotely sensed reflectance, $R_{rs}(\lambda)$, in order to obtain the modeled chlorophyll concentration, mChl-*a*. Then, mChl-*a* is compared with the in situ chlorophyll concentration data (Chl-*a*) to ascertain the algorithm's suitability for the region. Should discrepancies arise, we propose a regional adaptation of the algorithm.

The methodology unfolds in three phases. First, we describe the data, both $R_{rs}(\lambda)$, and in situ Chl-*a*. Subsequently, we describe the algorithms that transform $R_{rs}(\lambda)$ mChl-*a*. Lastly, we make an assessment of the algorithm using a comparison between the mChl-*a* and the in situ Chl-*a* data.

2.1. Remotely Sensed Reflectance Data

The satellite-derived surface reflectance data, $R_{rs}(\lambda)$, was obtained from Copernicus (<https://www.copernicus.eu/>). The Copernicus program has the objective of offering merged data records from multiple sensors (SeaWiFS, MODIS, MERIS, VIIRS-SNPP&JPSS1, OLCI-S3A&S3B) using the highest quality merging processes to date. Level 3 monthly averages of $R_{rs}(\lambda)$ at 412 nm, 443 nm, 490 nm, 555 nm and 670 nm wavebands, were retrieved for the area (Figure 1), that ranges from 23°N to 32°N in latitude and 120°W to 112°W in longitude. The composite images, with a resolution of 4 by 4 km, cover the period from January of 1998 to May of 2016 aligning with the collection dates of the in situ Chl-*a* data.

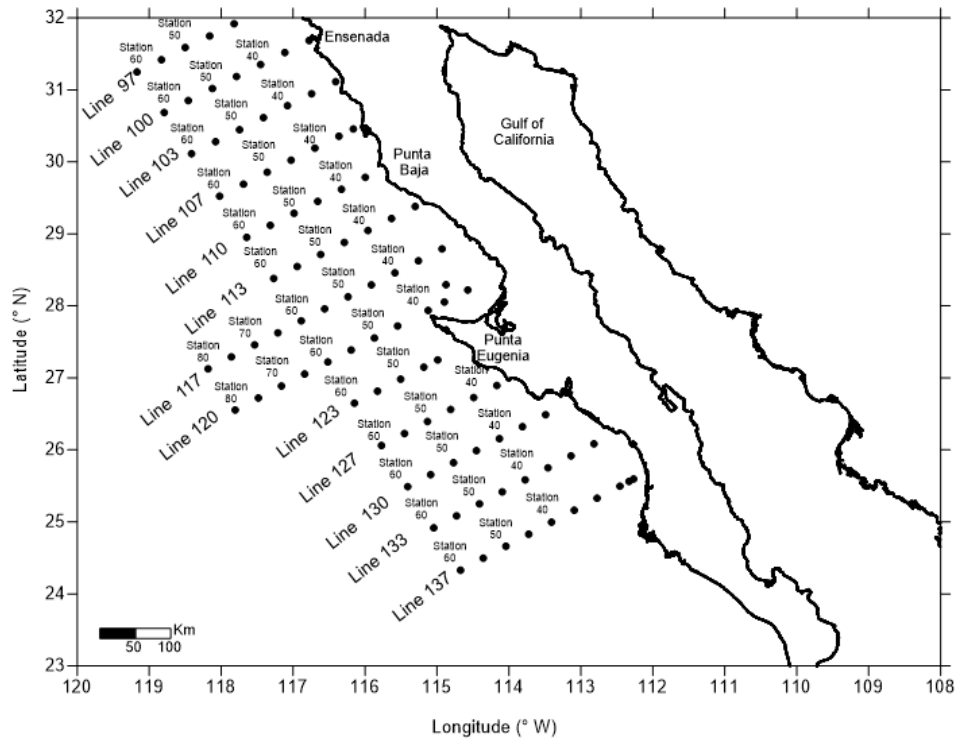


Figure 1. General grid of IMECOCAL stations where in situ samples were collected. The line number increases from 100 toward the South on line 137. Numbers above transects indicate station number which increases with distance from the coast.

2.2. In Situ Chlorophyll *a* Concentration Data

The in situ Chl-*a* concentration data belongs to the database collected from the IMECOCAL region (Figure 1) ranging from January 1998 to April 2016 (Table 1). To obtain the in situ Chl-*a*, water was collected from the network of stations, in 5 L Niskin bottles coupled in a rosette at varying depths: 1 m, 10 m, 20 m, 50 m, 100 m, 150 m and 200 m. Two liters of water at each depth were filtered through Whatman GF/F Filters at a pressure below 150 mm Hg. The filters were then placed in Histoprep tissue capsules (Fisherbrand) and frozen in liquid nitrogen pending analysis. Chlorophyll extraction was performed using acetone at 90% and at 4°C in darkness for 24 hours as recommended by [20]. Chl-*a* concentration (mg m^{-3}) was determined by the fluorometric method [21,22], with a Turner Designs A10 fluorimeter for the 1998 to 2005 samples and a Turner Designs trilogy fluorimeter for 2005 to 2016. Both fluorimeters were calibrated with pure Chl-*a* (Sigma). A more comprehensive description of the methodology can be found in [23]. For the purpose of this study, the mean in situ Chl-*a* concentration between the surface and 10 m depth data was used.

Table 1. Dates of IMECOCAL campaigns where in situ Chl-*a* data was obtained.

Year	January	February	March	April	May	June	July	August	September	October	November	December
1998												
1999												
2000												
2001												
2002												
2003												
2004												
2005												
2006												
2007												
2008												
2009												
2010												
2011												
2012												
2013												
2014												
2015												
2016												

2.3. Description of the Algorithms

Bio-optical algorithms are designed to estimate the near-surface chlorophyll-a concentration from satellite data by using a functional relationship between remotely sensed reflectance data, $R_{rs}(\lambda)$, and modeled chlorophyll-a concentration, mChl-a. These algorithms, developed since the 1970's, predominantly use empirical equations [9]. Among the plethora of available algorithms, the NASA Ocean Color website predominantly employs a combination of the O'Reilly band ratio (OCx) and the Hu Color index algorithm (CI) [10]. In addition to these global algorithms, there are specialized algorithms tailored for the California Current System, such as CalCOFI 2 [25]. This study will evaluate the efficacy of all the aforementioned algorithms within the IMECOCAL region.

2.3.1. OCx Algorithm

The OCx algorithm is one of the primary methodologies we employed to derive mChl-a from R_{rs} data. This algorithm is characterized by a polynomial relationship expressed as

$$\log_{10}(\text{mChl-a}) = a_0 + \sum_{i=1}^4 a_i F^i, \quad (1)$$

where the a_i coefficients of this function are sensor-specific and based on global data, [5,24], and F is the logarithm of the blue/green ratio of remotely sensed reflectances (\mathfrak{R}) as

$$F = \log_{10}[\mathfrak{R}] = \log_{10} \left[\frac{\max(Rrs(443,490))}{Rrs(555)} \right], \quad (2)$$

The OCx algorithm was assessed using the parameters associated with the different sensors (SeaWiFs, MERIS, MODIS and OCTS [24]). The optimal fit was for the SeaWiFs parameters $a_0 = 0.3272, a_1 = -2.9940, a_2 = 2.7218, a_3 = -1.2259, a_4 = -0.5683$. Consequently, these parameters were selected for this study.

2.3.2. CI algorithm

Another globally recognized algorithm explored in this study is the CI algorithm [10]. The CI algorithm employs a three-band model, utilizing reflectance values from the blue, green, and red bands (443 nm, 555 nm, and 670 nm, respectively):

$$CI = Rrs(555) - \left[Rrs(443) + \frac{555 - 443}{670 - 443} (Rrs(670) - Rrs(443)) \right], \quad (3)$$

This index is subsequently related to the mChl-*a* concentration through:

$$\log_{10}(\text{mChl-}a) = -0.409 + 191.6590 CI \quad (4)$$

The CI algorithm is employed for retrievals below 0.15 mg m⁻³, while the OCx algorithm is used for values exceeding 0.2 mg m⁻³. For intermediate values, a weighted combination of both algorithms is utilized [24].

2.3.3. CalCOFI 2 Algorithm

Given that our research data originates from the southern part of the CCS, we also considered algorithms specifically tailored for the California Current region. The CalCOFI 2 band linear algorithm [25] determines mChl-*a* using the logarithm of the blue/green ratio of reflectance, *F* (as defined in Equation (2)), in the following linear relationship:

$$\log_{10}(\text{mChl-}a) = 0.444F - 2.431 \quad (5)$$

2.4. Model Validation

To ensure the accuracy of our mChl-*a* model, we compared it against in situ Chl-*a* data. If discrepancies were observed, regional adjustments were proposed. For algorithm validation, we employed several metrics: the coefficient of determination R^2 , the adjusted coefficient of determination R_a^2 , the sum of squares error (SSE), and the root mean squared logarithmic error (RMSLE). Additionally, the Akaike information criterion (AIC) was computed to compare the modeled results:

$$AIC = -2\ln(L) + 2k \quad (6)$$

where *L* is the log-likelihood, and *k* is the number of parameters in the model [26].

3. Results

3.1. Performance of OCx, CI and CalCOFI 2 Algorithms

The performance of two global algorithms, OCx (Equation (12)) and CI (Equation (4)), alongside the CCS-specific CalCOFI 2 (Equation (5)), was assessed for the IMECOCAL region waters (Figure 2). All algorithms were applied to the reflectance data, yielding the logarithm of the mChl-*a* concentration. The results, plotted against *F* (Equation (2)), are shown in Figure 2. The CI algorithm exhibited greater dispersion in mChl-*a* estimates compared to OCx and CalCOFI 2. This is attributed to the CI algorithm's reliance on blue, green, and red bands (Equation (3)), whereas OCx and CalCOFI 2 utilize only the blue and green bands. This means that the CI algorithm has one more input variable than the others, therefore, there is greater dispersion on the resulting mChl-*a*.

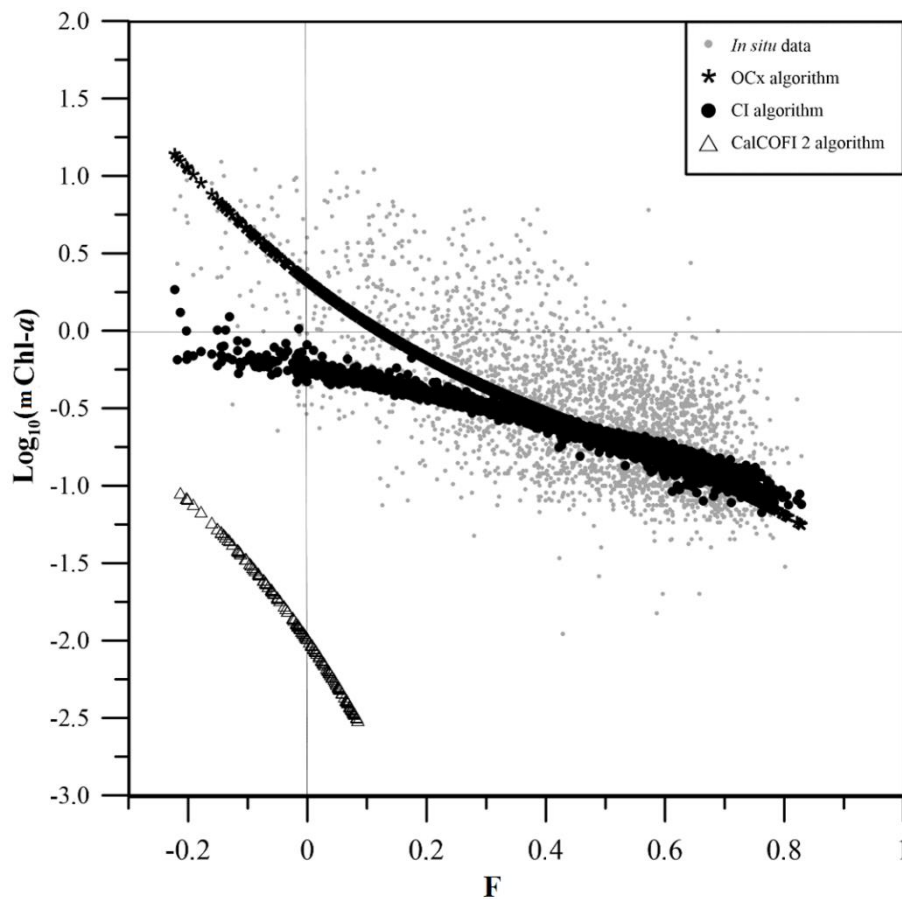


Figure 2. Results from applying OCx (asterisk), CI (circle), and CalCOFI2 (triangle) algorithms to remote sensing reflectance data ($F = \log_{10}[\mathfrak{R}]$, Equation (2)) off Baja California compared to the \log_{10} of in situ Chl-*a* data (grey circles).

As waters adopt a greener hue, F values decrease as $m\text{Chl-}a$ values increase. Upon applying the algorithms to the IMECOCAL data (Figure 2), the primary discrepancies between the OCx and CI algorithms correspond to values of $m\text{Chl-}a$ higher than or equal to 0.3 mg m^{-3} ($\log_{10}(m\text{Chl-}a) \sim -0.5$), and a ratio of blue/green reflectance of $\mathfrak{R} \leq 2.5$ ($F \leq 0.4$). For these reflectance ratios, OCx yields $m\text{Chl-}a$ values surpassing those of CI. The difference between CI and OCx retrievals for waters with large \mathfrak{R} values is small, yielding very similar results for the area though slightly higher retrievals for the CI algorithm.

The CalCOFI 2 algorithm consistently underestimated the chlorophyll concentration across the data spectrum. This underestimation increases with the value of the blue/green reflectance ratio \mathfrak{R} . Therefore, for the IMECOCAL area, OCx is the algorithm that yields the best results from a qualitative point of view. A comprehensive quantitative analysis will be presented subsequently. Based on both the qualitative and quantitative scrutiny of the algorithm retrievals, OCx is used as the basic algorithm for further comparisons, discarding the CI and CalCOFI 2 algorithms.

3.2. Performance of the Regionalized Algorithm Versus OCx

While the OCx algorithm aligns well with the region (Figure 2), refining it to better match the area's unique characteristics can enhance its accuracy. A polynomial fit was thus applied to model the functional relationship between F and the in situ Chl-*a* IMECOCAL data. Polynomial functions were tried because any function can be reduced to a polynomial through Taylor series. After evaluating polynomials from the first to the fifth order, the following fourth order function was selected based on quantitative metrics (R^2 , R^2_w , SSE, RMSLE and AIC).

$$\log(\text{mChl-}a) = 0.1746 - 1.9952F + 1.9992F^2 - 4.1958F^3 + 3.3837F^4 \quad (7)$$

Figure 4 shows the contrast between the in situ Chl-*a* data and the mChl-*a* derived from the OCx (global) and the regional algorithm (Equation (7)). The regional algorithm mChl-*a* values closely mirror those of the global algorithm within the $1.5 < \mathfrak{R} < 4.5$ ($0.18 < F < 0.65$) range of blue/green reflectance ratios. For values of $\mathfrak{R} > 4.5$ ($F > 0.65$), the regional algorithm estimates are approximately 1.8 mg m^{-3} higher than the global algorithm which is even larger than the CI retrievals (Figure 3). Conversely, for ratios $\mathfrak{R} < 1.5$ ($F < 0.18$), the regional algorithm yields lower mChl-*a*. Quantitatively, the regional algorithm consistently outperforms OCx, as evidenced by the SSE values for different *F* ranges. For the $F < 0.18$ area, the OCx sum of square error, SSE is of $24.4881 (\text{mg m}^{-3})^2$ while for the regional algorithm it is of $13.7582 (\text{mg m}^{-3})^2$. For the $F > 0.6$ region of the chart, SSE for OCx is $632.2217 (\text{mg m}^{-3})^2$ and for the regional algorithm it is $500.5084 (\text{mg m}^{-3})^2$. This indicates that the regional algorithm yields better results than the OCx.

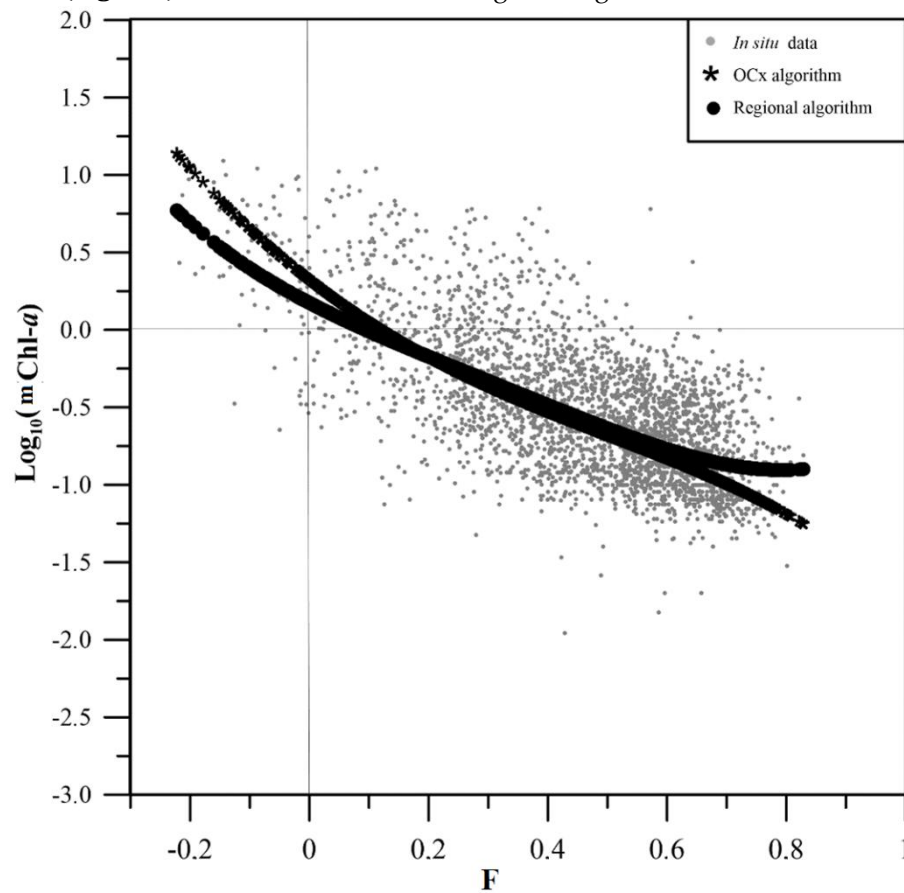


Figure 3. Regional (circles, Equation (7)) and OCx (asterisk) algorithm retrievals applied to remotely sensed reflectance data ($F = \log_{10}[\mathfrak{R}]$, Equation (2)) off Baja California compared to the \log_{10} of in situ Chl-*a* data (grey circles).

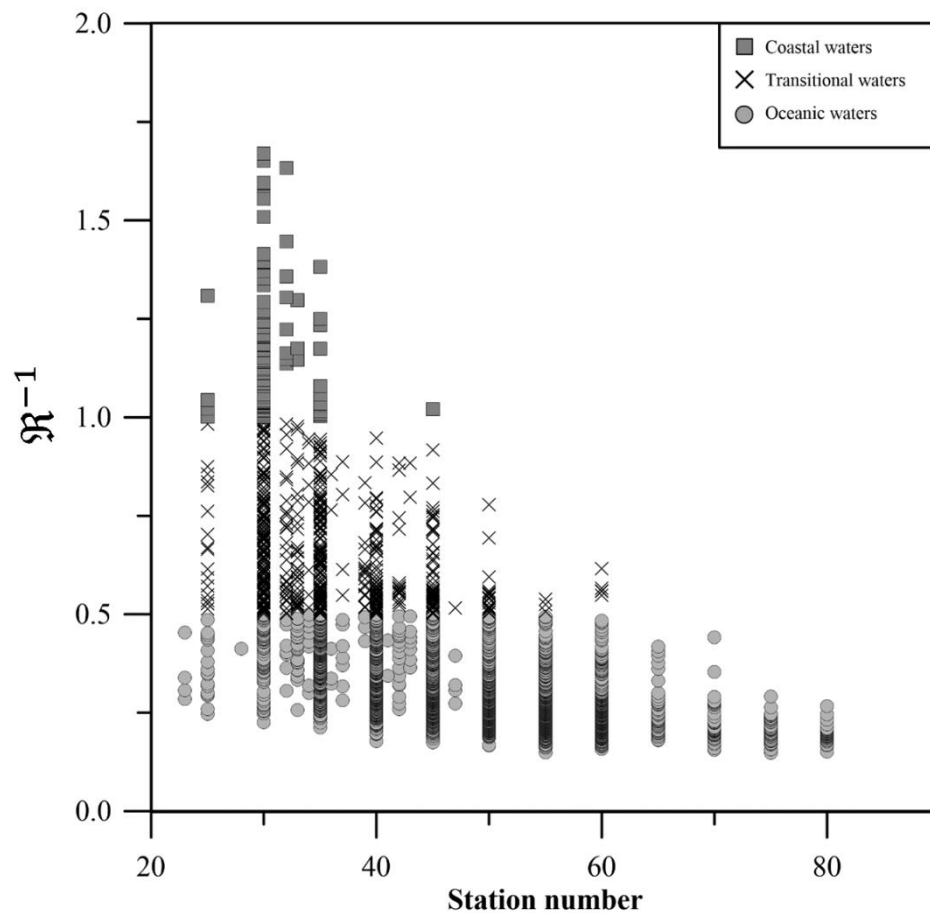


Figure 4. Variation of green/blue reflectance ratio (R^{-1}) with the station number (Figure 1) that increases with the distance from the coast. The stations were classified as: coastal waters with a green/blue ratio of reflectance of 1 and higher (squares, 105 stations), transitional waters with green/blue ratio between 0.5 and 1 (crosses, 653 stations), and oceanic waters with green/blue ratio of 0.5 and under (circles, 2607 stations).

3.3. Separating the Dataset

3.3.1. Dynamic Properties

In the vicinity of 32° N, water from the California Current (CC) converges with an intrusion of water from the Central North Pacific [27] thus, the CC turns toward the shore and part of it veers north to incorporate into the Southern California Eddy and the Southern California Countercurrent, while the remainder continues southward along the Baja California coast [28]. Therefore, this convergence forms a persistent feature called the Ensenada Front, an ecological transition zone [27] marked by a strong gradient in Chlorophyll-a concentration. In the Ensenada Front the eutrophic waters of the CC end abruptly, possibly due to the subduction of this pigment and nutrient rich waters to the southwest [28]. The Ensenada Front separates the CC region [28,29] in a northern mesotrophic area which has been studied by the CalCOFI project, and a southern oligotrophic area studied by the IMECOCAL project. As depicted in Figure 3, the CalCOFI 2 algorithm's performance underscores the need for distinct algorithms for these areas given the notably different bio-optical properties.

The southernmost part of the CCS, adjacent to the Baja California Peninsula, serves as a transitional zone where cold water from the subarctic meets warmer water coming from the tropics and subtropics [15,16]. The location of this transitional zone fluctuates seasonally [15] influencing the state of the oceanic ecosystem because circulation and water masses mixing, and convergence modulate the biological and chemical processes [17,18]. Previous studies ([15,18]) have identified two distinct provinces separated at around 28° N, at Punta Eugenia (Figure 1). North of Punta Eugenia

there are subarctic waters throughout most of the year, with year-round upwelling most intense during spring and early summer [16]. In the southern region coastal upwelling occurs mainly in spring and summer, while the tropical and subtropical influence is limited to summer and fall. Also, there are two cyclonic gyres: north and south of Punta Eugenia [15]. [16] suggested the separation in provinces is due to the change of sign in the wind stress curl at that latitude. This interruption in circulation has consequences in the biological properties of the area. Just as the Ensenada Front separates regions with markedly different bio-optical properties, this other dynamic boundary could have the same effect. Therefore, the dataset was separated to determine if these differences would yield an improvement in the mChl-*a* retrievals. The Southern province includes lines 123 to 137 and the Northern province includes lines 97 to 120, that is, North of Punta Eugenia (Figure 1). Despite expectations of differences in the distribution or values of \mathfrak{R} or mChl-*a*, the data dispersion was similar across both provinces, and the polynomials fitted (not shown) were almost the same and very similar to the regional algorithm proposed. Variance in mChl-*a* over the Northern province was $1.2583 (\text{mg m}^{-3})^2$ while in the Southern province was $1.1840 (\text{mg m}^{-3})^2$, with no statistical difference between the two areas.

3.3.2. Bio-Optical Properties

As with the latitudinal dynamic boundaries described before, coastal proximity is anticipated to influence Chlorophyll-*a* concentration due to various factors, including continental outflow of inorganic matter carried hundreds of miles from the coast by Santa Ana winds [30,31], upper layer mixing and thermocline shoaling originated by coastal upwelling, among others. These physical processes bring about nutrient enrichment in the euphotic zone and the subsequent increase of Chl-*a*. In order to explore the influence of near shore coastal processes and given the correlation between station number and proximity to the coast (Figure 1), the station number was plotted against the green/blue ratio, \mathfrak{R}^{-1} (Figure 4). A discernible pattern emerged with green/blue ratios higher than or equal to 1 nearer to the coast. This is likely due to the fact that these stations are nutrient-enriched and contain more Chl-*a* due to the photon absorption by the phytoplanktonic pigments [32]. When the green/blue ratio decreases, the mChl-*a* concentration also decreases. This offshore trend suggests that the data could be categorized based on bio-optical properties (green/blue reflectance ratio) in three categories: (a) coastal waters with a green/blue ratio of reflectance of 1 and higher, (b) transitional waters with green/blue ratio between 0.5 and 1, and (c) oceanic waters with green/blue ratio of 0.5 and lower.

Polynomial algorithms were then fitted for each category (Figure 5), with the order determined by quantitative analysis metrics (R^2 , R_a^2 , SSE, RMSLE and AIC)

$$\log_{10}(\text{mChl-}a) = 0.2138 - 2.6481F \quad (8)$$

$$\log_{10}(\text{mChl-}a) = 0.2501 - 1.7957F - 0.4325F^2 \quad (9)$$

$$\log_{10}(\text{mChl-}a) = 0.2786 - 2.1925F + 0.8474F^2 \quad (10)$$

The results of these algorithms, depicted in Figure 5, align with the general data trend and closely resemble the regional algorithm (lower mChl-*a* prediction than OCx for coastal waters (small \mathfrak{R} , large \mathfrak{R}^{-1}) and higher mChl-*a* predictions than OCx for oceanic waters (small \mathfrak{R}^{-1})). These algorithms consider the bio-optical properties of each area: coastal stations have greater abundance of microphytoplankton (diatoms, dinoflagellates, silicoflagellates) associated to a larger phytoplanktonic absorption coefficient whereas in oceanic waters smaller phytoplanktonic cells are found (nano and picophytoplankton) with smaller absorption coefficients [33]. They, also, offer the advantage of simpler inversion and reduced overfitting risk. The regional algorithm, on the other hand, provides a unified function for the entire \mathfrak{R} range.

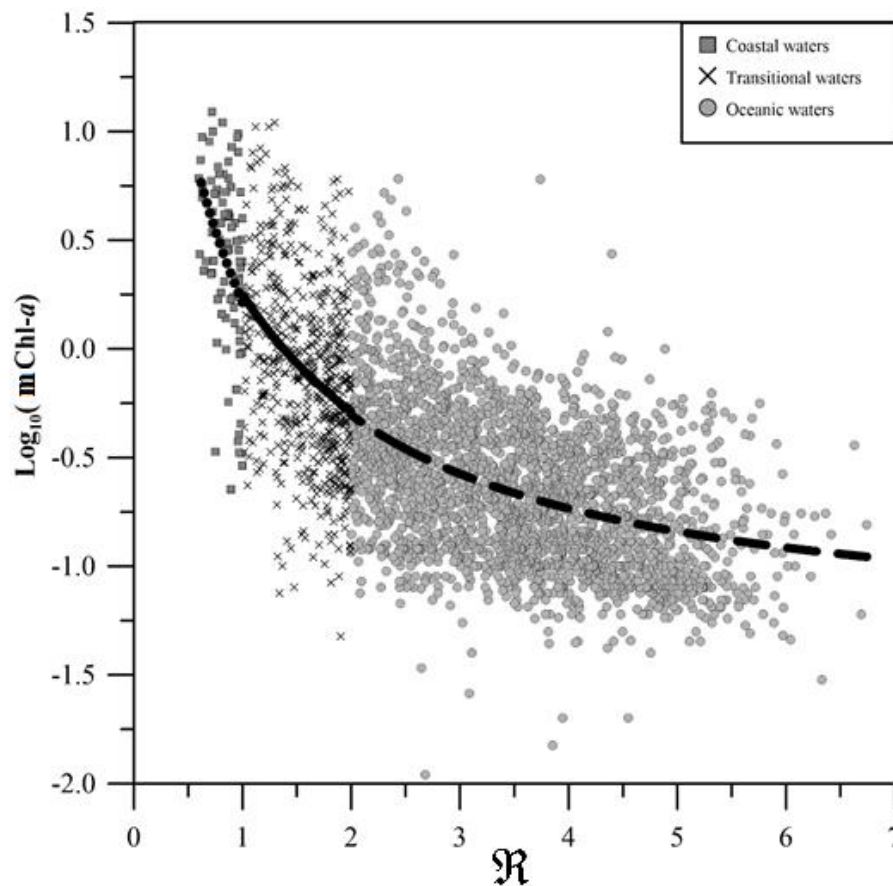


Figure 5. Retrievals of \log_{10} of mChl-*a*, using Equation (8), for coastal waters (dotted line), Equation (9) for transitional waters (solid line), and Equation (10) for oceanic waters (dashed line), compared to the \log_{10} of in situ Chl-*a* data (square for coastal waters, cross for transitional waters, and circles for oceanic waters).

3.3.3. Climatic Events

In addition to the dynamic and bio-optical properties, it is crucial to consider the impact of large-scale climatic events on the region's properties. Notably, discrepancies have been observed during ENSO events in the CCS [29]. The shifting boundaries between subarctic waters and tropical/subtropical waters during cold and warm events have been identified [18]. Such shifts, generally associated with changes in circulation, biological, and chemical characteristics, necessitate an analysis of in situ data variations during these events.

To classify the data, three distinct indexes were employed: the Southern Oscillation Index (SOI, <https://www.ncdc.noaa.gov/>), the Oceanic Niño Index (ONI, <https://origin.cpc.ncep.noaa.gov/>), and the multivariate ENSO index (MEI, <https://www.esrl.noaa.gov/>). Data was categorized as El Niño, or La Niña based on the classification provided by any of the three indexes for the respective month and year. If none of the indexes indicated a cold or warm event for that period, the data was labeled as normal. Subsequently, a polynomial function was fitted for each condition, as depicted in Figure 6.

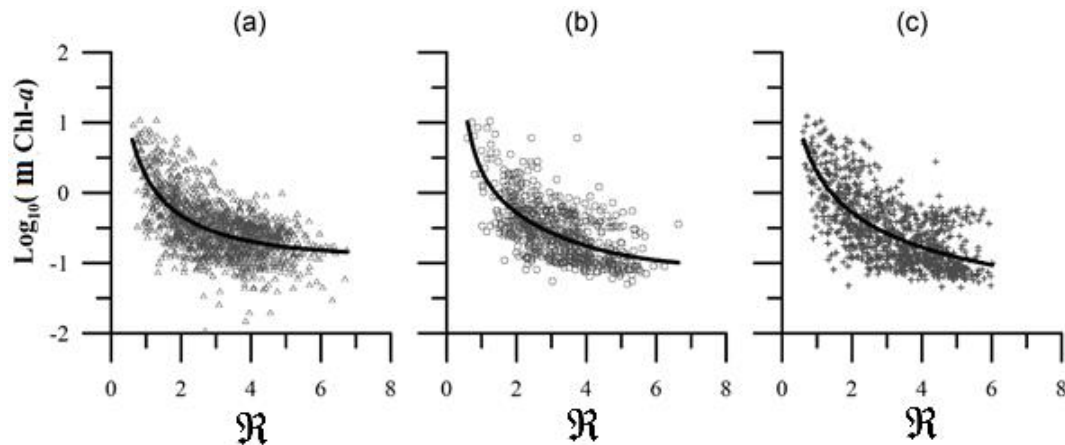


Figure 6. Algorithm retrievals for data classified as: (a) La Niña; (b) El Niño; (c) normal compared to the \log_{10} of in situ Chl-*a* data.

In waters off the Baja California Peninsula coastal upwelling determines the variability of the phytoplankton community [34]. Therefore, when there is a disruption in these patterns, i.e. during El Niño/La Niña events, biomass and community composition experience a shift. A warm El Niño event is usually associated with weaker alongshore northwesterly winds, deepening of the seasonal thermocline, as well as with the near shore poleward transport of warmer, nutrient depleted water. Therefore, a decrease in diatom abundance and an increase in the small cell communities is expected. A cold La Niña event brings stronger winds and colder, nutrient rich water which tend to favor diatom growth [35,36].

[29] analyzed the extent of eutrophic and mesotrophic areas of the California Current during ENSO events and observed important differences between the waters off Baja California to those off California. [29] noted a reduction of the eutrophic and mesotrophic areas off the Southern California Bight associated to a decrease in upwelling; also, there was an increase in the extent of the mesotrophic areas off Baja California extending up to 700 km offshore, thus, not likely due to upwelling but, possibly to cyanobacteria. During the El Niño event of 1997-1998, [37] noted that in the region South of Punta Eugenia, tropical and subtropical waters dominated the region, while North of Punta Eugenia there was a coastal poleward flow that displaced the core of the California Current offshore. Due to the large variability of this transitional region, both at the seasonal and interannual scales, one would not expect a global algorithm to adequately comprise the processes within this ecosystem.

The analysis for interannual warm and cold events in Figure 6 revealed that most data have high R values and low Chlorophyll-*a* during El Niño. Therefore, during El Niño events, waters tend to be more oligotrophic, showing the expected shift towards smaller cells [36]. This is because warmer waters make both thermocline and nutricline deeper, diminishing nutrient availability in the euphotic zone [38]. Also, different behaviors can be seen with the simplest algorithm for the normal (Equation (11)) and La Niña (Equation (12)) data and the more complex for El Niño events (Equation (13)). The algorithms developed for different climatic conditions, as detailed in Equations (13)–(15), were selected based on quantitative analysis metrics (R^2 , R_a^2 , SSE, RMSLE and AIC, see Table 2 below)

$$\log_{10}(\text{mChl-}a) = 0.2962 - 2.0437F + 0.4425F^2 \quad (11)$$

$$\log_{10}(\text{mChl-}a) = 0.2337 - 2.1695F + 1.0492F^2 \quad (12)$$

$$\log_{10}(\text{mChl-}a) = 0.3141 - 2.4323F + 2.2698F^2 - 3.1653F^3 + 2.0039F^4 \quad (13)$$

Table 2. The coefficient of determination (R^2), the adjusted coefficient of determination (R_a^2), the sum of square error (SSE), the root mean squared logarithmic error (RMSLE) and the Akaike information criterion (AIC) for each of the tested and proposed algorithms. The R^2 and R_a^2 marked with an asterisk were outside of the expected range of [0,1].

Error	CalCOFI 2	CI	OCx	Regional	Bio-optical properties	Climatic condition
SSE	156,141.81	450.60	364.03	340.33	338.39	331.52
R^2	0*	0.2640	0.4054	0.4441	0.4473	0.4585
R_a^2	0*	0.2637	0.4046	0.4434	0.4465	0.4579
AIC	25,949.82	8,195.45	7,553.75	7,349.37	7,332.03	7,267.75
RMSLE	7.1715	0.3853	0.3463	0.3348	0.3339	0.3304

3.4. Quantitative Comparison of Algorithms

The performance of each algorithm was evaluated using various error metrics, as outlined in Equations (6)–(8), with the results presented in Table 2. The CalCOFI 2 algorithm exhibited the highest error, confirming its unsuitability for waters off Baja California. In contrast, the OCx algorithm outperformed the CI algorithm, as evidenced by the SSE values. The algorithm considering climatic conditions demonstrated the most promising results, with the lowest values for SSE, RMSLE, and AIC. The difference between the coefficient of determination and its adjusted value depends on the degrees of freedom and is reflected in the third decimal number, indicating that the differences are not important and, therefore, can be considered the same. The RMSLE and the SSE are lowest for the algorithm with the climatic condition. The regional algorithm, while an improvement over the global algorithms tested, was further enhanced when the dataset was segmented based on bio-optical properties and climatic conditions.

4. Discussion

The applicability of global algorithms to the waters off the Baja California Peninsula was assessed. Both CI and OCx algorithms exhibit similarities for waters with mChl-*a* values less than 0.3 mg m⁻³ ($\log_{10}(\text{mChl-}a) \sim -0.5$) and a blue/green reflectance ratio of $\mathfrak{R} \geq 2.5$ ($F \geq 0.4$) as depicted in Figure 2. While CI is deemed superior for retrievals below 0.15 mg m⁻³, OCx is more effective for higher mChl-*a* concentrations ($\text{Chl-}a \geq 0.2$ mg m⁻³) [24]. Given the natural data dispersion surpasses the difference between CI and OCx for mChl-*a* < 0.3 mg m⁻³, OCx was deemed more suitable for the region, leading to its selection for regionalization.

The proposed regional algorithm demonstrates a superior fit for the area compared to OCx, as evidenced in Table 2. A comparison of the data (Figure 3) highlights the divergence between algorithms, particularly in extreme conditions of oligotrophic (high \mathfrak{R} or *F*, low mChl-*a*) and eutrophic waters (low \mathfrak{R} or *F*, high mChl-*a*). This discrepancy suggests that the IMECOCAL region's oligotrophic waters possess a higher pigment concentration than the global database used to derive OCx parameters. As [28] posits, the presence of small cells (cyanobacteria), typical of tropical and subtropical waters in warm waters off the Baja California Peninsula, could explain this variation. While other factors like particulate matter or continental debris might influence this difference, their sporadic occurrence means their impact is limited to specific situations and data points. As per [5], OCx is effective in eutrophic areas due to its higher mChl-*a* output. However, the IMECOCAL region's data indicates lower mChl-*a* values for smaller \mathfrak{R} values, leading the regional algorithm to produce reduced mChl-*a* results. This suggests the eutrophic zone in the IMECOCAL region has a lower pigment concentration than the global database.

The regional algorithm, tailored to the unique oceanographical and optical properties of the area, offers improved predictions for both eutrophic and oligotrophic zones. The segmentation of the database resulted in models with minimal complexity (Equation (10) through 12). Notably, a linear model was the best fit for coastal waters (Figure 6). The most optimal overall fit was achieved when the database was segmented based on climatic conditions. The El Niño condition presents a more

intricate data distribution compared to La Niña and normal conditions. During La Niña events, the colder waters and intensified upwelling [18] enhance nutrient availability for phytoplankton, thereby elevating mChl-*a* levels, predominantly in coastal and transitional stations. Such events alter the region's physical, biological, and chemical attributes, promoting microphytoplankton growth. The consequential shift in the phytoplankton community, as reflected in the algorithms, underscores the climatic conditions' significance for the region.

5. Conclusions

The Chlorophyll-*a* satellite images are one of the most used products in oceanography [39]. However, the global algorithms applied are biased because their parameters are obtained with data from all around the globe and for a particular sensor. Therefore, it is important to assess their efficiency in order to determine if they are regionally appropriate before its use [39]. When applied to the IMECOCAL area with the Copernicus satellite data, the two global algorithms (OCx and CI) yielded results within the range of in situ Chl-*a* values expected. Because it includes information of reflectance at 670 nm [10], the CI algorithm produces mChl-*a* values with more dispersion than the OCx. However, for the IMECOCAL area the difference between the results of the CI and OCx algorithms is so slight that the change in algorithm does not warrant improvement in the mChl-*a* estimates.

Off California, the global algorithms underestimate the Chlorophyll-*a* concentration by a factor of 5 [2,6]. However, for the IMECOCAL area these algorithms retrieved mChl-*a* of the same order of magnitude as the in situ Chl-*a* data. The CalCOFI 2 algorithm, on the contrary, drastically underestimates the in situ Chl-*a* concentration in the IMECOCAL area, suggesting that there are significantly different bio-optical properties between these sections of the CC. The fact that the Ensenada Front works as a dynamic boundary that greatly alters the bio-optical properties in different sections of the CCS suggests that the boundary at around 28° N [15] that reduces ecological connectivity would do the same. Nonetheless, the data are not significantly different showing that this dynamic boundary does not have a perceptible effect in the bio-optical properties of seawater in the area. The differences observed in the algorithms could be due, not only to the bio-optical differences in the data per se but to the differences in the merged satellite data. Therefore, it is important to establish accurate parameters for the specific merged satellite data.

The regional algorithm differs from the global OCx mainly in oligotrophic waters, with higher Chlorophyll-*a* values that could be due to the presence of small cells characteristic of tropical and subtropical waters. The database was then classified according to the green/blue ratio of reflectances (R^{-1}) which allowed a distinction between coastal, transitional, and oceanic waters, each with a polynomial function fitted to it. Though the differences between the regional algorithm and this set of algorithms are small, the classification in coastal, transitional, and oceanic waters allows a better parameterization for different properties as with the combined use of CI and OCx by NASA. The weighed approach used for CI and OCx is based on Chl-*a* value, which requires a retrieval for the determination of the adequate algorithm. The use of this set allows a distinction of properties based on a value of R , that is, the classification of the data is done before the retrieval.

During El Niño events, Chlorophyll-*a* was lower than during the transitional and La Niña conditions. When analyzing the interannual variations associated with ENSO, [40] found an increase in the mesotrophic area in the IMECOCAL region during these warm events. This coincides with the fact that for the IMECOCAL area, the dispersion in R values are less during an El Niño. [41] found that during the cold event of 2008 the productivity rates increased. This coincides with the high Chlorophyll-*a* observed in the IMECOCAL data during La Niña and normal conditions than during an El Niño.

[39] stated that regionalizing the algorithms diminishes the bias, but uncertainties are still important because of the natural variation of the optical properties of phytoplankton, the presence of other optically active components, and the atmospheric correction. These authors found that removing the 443 nm band improved the performance of the OCx algorithm. There is still much work to do in order to give a more accurate estimate of mChl-*a* from satellite data. However, the evaluation

of the algorithms using merged satellite data gives a deeper understanding of the area and a better option for constructing long time-series that can aid in the comprehension of the processes in the area. With the Copernicus satellite data, the climatic conditions algorithm allows the construction of more consistent time series for the IMECOCAL region.

Author Contributions: Conceptualization, Patricia Alvarado-Graef and Beatriz Martin-Atienza; Data curation, Ramón Sosa-Ávalos; Formal analysis, Patricia Alvarado-Graef and Beatriz Martin-Atienza; Investigation, Patricia Alvarado-Graef and Ramón Sosa-Ávalos; Methodology, Patricia Alvarado-Graef, Beatriz Martin-Atienza, Ramón Sosa-Ávalos and Rafael Hernández-Walls; Resources, Reginaldo Durazo; Software, Patricia Alvarado-Graef; Supervision, Beatriz Martin-Atienza; Writing – original draft, Patricia Alvarado-Graef; Writing – review & editing, Beatriz Martin-Atienza, Ramón Sosa-Ávalos, Reginaldo Durazo and Rafael Hernandez-Walls.

Funding: Patricia Alvarado-Graef received a scholarship from SEP-PRODEP project: “Fortalecimiento de Cuerpos Académicos” convocatoria 2018.

Conflicts of Interest “The authors declare no conflict of interest.”

References

1. Maritorena, S.; Siegel, D. A. Consistent merging of satellite ocean color data sets using a bio-optical model. *Remote Sensing of Environment*. **2005**, *94*, 429-440. <https://doi.org/10.1016/j.rse.2004.08.014>
2. Kahru, M.; Kudela, R. M.; Anderson, C. R.; Mitchell, B. G. Optimized merger of ocean chlorophyll algorithms of MODIS-Aqua and VIIRS. *IEEE Geoscience and Remote Sensing Letters*. **2015**, *12*(11), 2282-2285. <https://doi.org/10.1109/lgrs.2015.2470250>
3. O'Reilly, J.E.; Werdell, P.J. Chlorophyll algorithms for ocean color sensors – OC4, OC5 & OC6. *Remote Sensing of Environment*. **2019**, *229*, 32-47. <https://doi.org/10.1016/j.rse.2019.04.021>
4. McClain, C. R. A decade of satellite ocean color observations. *Annual Review of Marine Science*. **2009**, *1*, 19-42. <https://doi.org/10.1146/annurev.marine.010908.163650>
5. O'Reilly, J. E.; Maritorena, S.; O'Brien, M.C.; Siegel, D.A.; Toole, D.; Menzies, D.; Smith, R.C.; Mueller, J.L.; Mitchell, B.G.; Kahru, M.; Chavez, F.P.; Strutton, P.; Cota, G.F.; Hooker, S.B.; McClain, C.R.; Carder, K.L.; Müller-Karger, F.; Harding, L.; Magnuson, A.; Phinney, D.; Moore, G.F.; Aiken, J.; Arrigo, K.R.; Letelier, R.; Culver, M. Vol. 11, SeaWiFS Postlaunch Calibration and Validation Analyses, Part 3. In: Hooker, S. B., Firestone, E. R. (Eds.), *NASATech. Memo. 2000- 206892*. NASA Goddard Space Flight Center. **2000**, 49 pp.
6. Kahru, M.; Kudela, R. M.; Manzano-Sarabia, M.; Mitchell, B.G. Trends in the surface chlorophyll of the California Current: Merging data from multiple ocean color satellites. *Deep-Sea Research Part II: Topical Studies in Oceanography*. **2012**, *77*–80, 89-98. <https://doi.org/10.1016/j.dsr2.2012.04.007>
7. IOCCG. Ocean-color data merging. In: Gregg, W. (Ed.), *Report of the International Ocean-Color Coordinating Group*; IOCCG, Dartmouth, Canada, No.6. **2007**. 68 pp.
8. Groom, S.; Sathyendranath, S.; Ban, Y.; Bernard, S.; Brewin, R.; Brotas, V.; Brockmann, C.; Chauhan, P.; Choi, J.K.; Chuprin, A.; Ciavatta, S.; Cipollini, P.; Donlon, C.; Franz, B.; He, X.; Hirata, T.; Jackson, T.; Kampel, M.; Krasemann, H.; Lavender, S.; Pardo-Martinez, S.; Mélin, F.; Platt, T.; Santoleri, R.; Skakala, J.; Schaeffer, B.; Smith, M.; Steinmetz, F.; Valente, A.; Wang, M. Satellite Ocean Colour: Current Status and Future Perspective. *Frontiers in Marine Science*. **2019**, *6*, 1-30. <https://doi.org/10.3389/fmars.2019.00485>
9. O'Reilly, J.E.; Maritorena, S.; Mitchell, B.G.; Siegel, D.A.; Carder, K.L.; Garver, S.A.; Kahru, M.; McClain, C. Ocean color chlorophyll algorithms for SeaWiFS. *Journal of Geophysical Research: Oceans*. **1998**, *103*, 24937-24953. <https://doi.org/10.1029/98JC02160>
10. Hu, C.; Lee, Z.; Franz, B. Chlorophyll *a* algorithms for oligotrophic oceans: A novel approach based on three-band reflectance difference. *Journal of Geophysical Research: Oceans*. **2012**, *117*, C01011, 1-25. <https://doi.org/10.1029/2011JC007395>
11. Kahru, M.; Kudela, R.M.; Anderson, C.R.; Manzano-Sarabia, M.; Mitchell, B.G. Evaluation of satellite retrievals of ocean chlorophyll-a in the California Current. *Remote Sensing*. **2014**, *6*(9), 8524-8540. <https://doi.org/10.3390/rs6098524>
12. Lee, S.H.; Ryu, J.; Park, J.; Lee, D.; Kwon, J.; Zhao, J.; Son, S. Improved Chlorophyll-a Algorithm for the Satellite Ocean Color Data in the Northern Bering Sea and Southern Chukchi Sea. *Ocean Science Journal*. **2018**, *53*, 475-485. <https://doi.org/10.1007/s12601-018-0011-5>
13. Mustapha, S.B.; Bélanger, S.; Larouche, P. Evaluation of ocean color algorithms in the southeastern Beaufort Sea, Canadian Arctic: New parameterization using SeaWiFS, MODIS, and MERIS spectral bands. *Canadian Journal of Remote Sensing*. **2012**, *38*(5), 535-556. <https://doi.org/10.5589/m12-045>
14. Kurian, J.; Colas, F.; Capet, X.; McWilliams, J.C.; Chelton, D.B. Eddy properties in the California Current System. *Journal of Geophysical Research: Oceans*. **2011**, *116*, C08027, 1-18. <https://doi.org/10.1029/2010JC006895>

15. Durazo, R.; Ramírez Manguilar, A.M.; Miranda, L.E.; Soto Mardones, L.A. Climatología de variables oceanográficas. In: Gaxiola Castro G, Durazo R (eds.), *Dinámica del ecosistema pelágico frente a Baja California 1997-2007*. SEMARNAT, CICESE, UABC, **2010**, 25-58. Available (in Spanish) from: <https://imecocal.cicese.mx/wp/wp-content/uploads/Durazo-Gaxiola-2010.pdf>, July 12, 2023.
16. Durazo, R. Seasonality of the transitional region of the California Current System off Baja California. *Journal of Geophysical Research: Oceans*. **2015**, 120, 1173-1196. <https://doi.org/10.1002/2014JC010405>
17. Gaxiola-Castro, G.; Durazo, R.; Lavaniegos, B.; De La Cruz-Orozco, M.E.; Millán-Núñez, E.; Soto-Mardones, L.; Cepeda-Morales, J. Pelagic ecosystem response to interannual variability off Baja California. *Ciencias Marinas*. **2008**, 34(2), 263-270. <https://doi.org/10.7773/cm.v34i2.1413>
18. Durazo, R. Climate and upper ocean variability off Baja California, Mexico: 1997–2008. *Progress in Oceanography*. **2009**, 83(1–4), 361-368, <https://doi.org/10.1016/j.pocean.2009.07.043>
19. Boyce, D.G.; Lewis, M.R.; Worm, B. Global phytoplankton decline over the past century. *Nature*. **2010**, 466, 591-596. <https://doi.org/10.1038/nature09268>
20. Venrick, E.L.; Hayward, T.L. Determining chlorophyll on the 1984 CalCOFI surveys. *CalCOFI Reports*. **1984**, 25, 74.
21. Holm-Hansen, O.; Lorenzen, C.J.; Holmes, R.W.; Strickland, J.D.H. Fluorometric determination of chlorophyll. *ICES Journal of Marine Science*. **1965**, 30(1), 3-15. <https://doi.org/10.1093/icesjms/30.1.3>
22. Yentsch, C.S.; Menzel, D. W. A method for the determination of phytoplankton, chlorophyll and phaeophytin by fluorescence. *Deep-Sea Research*. **1963**, 10, 221-231.
23. De la Cruz-Orozco, M. E.; Gómez-Ocampo, E.; Miranda-Bojórquez, L.E.; Cepeda-Morales, J.; Durazo, R.; Lavaniegos, B.E.; Espinosa-Carreón, T.L.; Sosa-Avalos, R.; Aguirre-Hernández, E.; Gaxiola-Castro, G. Phytoplankton biomass and production off the Baja California Peninsula: 1997 – 2016. *Ciencias Marinas*. **2017**, 43(4), 217-228. <https://doi.org/10.7773/cm.v43i4.2793>
24. NASA. (2010). *SeaWiFS Project online*. Seattle (WA, USA): NASA. Available online: <https://oceancolor.gsfc.nasa.gov/SeaWiFS/> (accessed on 09/10/2019).
25. Mitchell, B.G.; Kahru, M. Algorithms for SeaWiFS standard products developed with CalCOFI bio-optical data. *CalCOFI Reports*. **1998**, 39, 133-147.
26. Burnham, K.P.; Anderson, D.R. Model Selection and Multimodel Inference: A Practical Information-Theoretic Approach, 2nd Edition, Springer-Verlag, U.S.A. **2002**, 488 pp.
27. Venrick, E.L. Summer in the Ensenada Front: The distribution of phytoplankton species, July 1985 and September 1988. *Journal of Plankton Research*. **2000**, 22(5), 813-841. <https://doi.org/10.1093/plankt/22.5.813>
28. Haurly, L. R.; Venrick, E.L.; Fey, C.L.; McGowan, J.A.; Niiler, P.P. The Ensenada Front. *CalCOFI Reports*. **1993**, 34, 69-88.
29. Kahru, M.; Mitchell, B. G. Influence of the 1997-98 El Niño on the surface chlorophyll in the California Current. *Geophysical Research Letters*. **2000**, 27(18), 2937-2940. <https://doi.org/10.1029/2000GL011486>
30. Castro, R.; Parés-Sierra, A.; Marinone, S.G. Evolución y extensión de los vientos Santa Ana de febrero de 2002 en el océano, frente a California y la península de Baja California. *Ciencias Marinas*. **2003**, 29(3), 275-281. <https://doi.org/10.7773/cm.v29i3.158>
31. Sosa-Ávalos, R.; Gaxiola-Castro, G.; Durazo, R.; Mitchell, B. G. Effect of Santa Ana winds on bio-optical properties off Baja California. *Ciencias Marinas*. **2005**, 31(2), 339-348. <https://doi.org/10.7773/cm.v31i2.60>
32. Falkowski, P. G.; Raven, J. A. *Aquatic Photosynthesis*. Second Edition. Princeton University Press. **2007**. 484 pp.
33. Alvarado-Graef, P.; Martín-Atienza, B; Sosa-Ávalos, R.; Durazo, R. An Ocean Color Algorithm Based on Power Functions to Retrieve Inherent Optical Properties from Remotely Sensed Data Off the Baja California Peninsula, Mexico. *IEEE Transactions on Geoscience and Remote Sensing*. **2020**, 58(3), 1868-1876. <https://doi.org/10.1109/TGRS.2019.2949946>
34. Gaxiola, G.; Cepeda-Morales, J.; Nájera-Martínez, S.; Espinosa-Carreón, T.L.; De la Cruz-Orozco, M.E.; Sosa-Avalos, R.; Aguirre-Hernández, E.; Cantú-Ontiveros, J.P. Biomasa y producción del fitoplancton. In: Gaxiola-Castro G, Durazo R (eds.), *Dinámica del ecosistema pelágico frente a Baja California 1997-2007*. SEMARNAT, CICESE, UABC. **2010**, pp. 59–86.
35. Moran, X.A.G.; López-Urrutia, A.; Calvo-Díaz, A.; Li, W.K.W. Increasing importance of small phytoplankton in a warmer ocean. *Global Change Biology*. **2010**, 16(3), 1137-1144. <https://doi.org/10.1111/j.1365-2486.2009.01960.x>
36. González-Silvera, A.; Santamaría-del-Ángel, E.; Camacho-Ibar, V.; López-Calderón, J.; Santander-Cruz, J.; Mercado-Santana, A. The Effect of Cold and Warm Anomalies on Phytoplankton Pigment Composition in Waters off the Northern Baja California Peninsula (México): 2007–2016 *Journal of Marine Science and Engineering*. **2020**, 8, 533; <https://doi.org/10.3390/jmse8070533>
37. Durazo, R.; Baumgartner, T. Evolution of oceanographic conditions off Baja California: 1997–1999. *Progress in Oceanography*. **2002**, 54, 7-31. <https://doi.org/10.1016/S0079-6611%2802%2900041-1>
38. Mann, K. H.; Lazier, J. R. *Dynamics of Marine Ecosystems. Biological-Physical Interactions in the oceans*. Third edition. Blackwell Publishing. **2006**. 496 pp.

39. Clay, S.; Peña, A.; DeTracey, B.; Devred, E. Evaluation of Satellite-Based Algorithms to Retrieve Chlorophyll-a Concentration in the Canadian Atlantic and Pacific Oceans. *Remote Sensing*. **2019**, 11(2), 2609. <https://doi.org/10.3390/RS11222609>
40. Kahru, M.; Mitchell, B. G. Empirical chlorophyll algorithm and preliminary SeaWiFS validation for the California Current. *International Journal of Remote Sensing*. **1999**, 20(17), 3423-3429. <https://doi.org/10.1080/014311699211453>
41. Gómez-Ocampo, E.; Gaxiola-Castro, G.; Durazo, R.; Beier, E. Effects of the 2013-2016 warm anomalies on the California Current phytoplankton. *Deep-Sea Research Part II: Topical Studies in Oceanography*. **2018**, 151, 64-76. <https://doi.org/10.1016/j.dsr2.2017.01.005>

Disclaimer/Publisher's Note: The statements, opinions and data contained in all publications are solely those of the individual author(s) and contributor(s) and not of MDPI and/or the editor(s). MDPI and/or the editor(s) disclaim responsibility for any injury to people or property resulting from any ideas, methods, instructions or products referred to in the content.